24AM1A-06

Electromagnetic Wave Scattering from Lossy Polygonal Cylinders

An N. Nguyen [#1], Hiroshi Shirai[#2]

[#] *Graduate School of Science and Engineering, Chuo University*
1-13-27 Kasuga, Bunkyo-ku, Tokyo, 112-8551, Japan

[1] ngocanvnn@shirai.elect.chuo-u.ac.jp

[2] shirai@elect.chuo-u.ac.jp

Abstract—**In order to study the electromagnetic scattering properties of lossy dielectric polygonal body, Kirchhoff's approximation was used to derive scattering far-field components. Numerical calculations were carried out for some lossy dielectric and metallic rectangular cubes at different frequencies, and then they were compared to measured radar cross section data in order to verify the validity of our approximation. Good agreements were observed in specular reflection directions, especially in the case of electrically large metal cube.**

I. INTRODUCTION

For several decades, topics on electromagnetic scattering have been widely studied with various shapes and models using rigorous analytical calculation in some cases and approximation method in the other cases. With regards to material, knowledge about scattering properties at high frequencies of objects made of lossy material is of paramount importance in radar applications, anti-radar designs, and high frequency electronic device manufacture [1, 2]. From high frequency scattering properties of object, critical information about unknown characteristics of the object, like complex relative permittivity, shape and dimensions, can be extracted and used in different purposes such as target reconstruction, target detection, and dielectric constant measuring.

In this research, we present an approximate solution in order to determine scattering fields from polygonal bodies made of lossy material. Since any smooth curve can be approximated by a sufficient number of finite surfaces, we may extend the results for arbitrarily shaped objects. Because there is no existing analytical solution to diffraction at lossy dielectric wedges, we used Kirchhoff's approximation to calculate theoretically. However, this estimation is valid only when the wavelength is small enough in comparison with the object's dimensions.

Asymptotic approximation method has been used to derive the scattering far-fields, and their results are utilized to obtain radar cross section. Finally, in order to verify the validity of this approximation, theoretically calculated radar cross section and measured data of some lossy dielectric and metal cubes were compared. Time harmonic factor $e^{-i\omega t}$ is assumed and suppressed throughout the context.

II. FORMULATIONS

Let us consider, as shown in Fig.1, a H-polarized plane wave:

$$H_z^i = e^{-ikx\cos\theta_0 - iky\sin\theta_0} \quad (1)$$

impinges upon a lossy dielectric polygonal cylinder, whose permittivity and cross section are assumed to be $\varepsilon = \varepsilon_r\varepsilon_0$ and $2a\times 2b$, respectively. k $(= 2\pi/\lambda)$ is the wave number and λ is the wavelength in free space.

When the size $(2a\times 2b)$ is large compared with the wavelength, the scattering field can be estimated accurately by high frequency asymptotic technique. It is already known that the Geometrical Theory of Diffraction (GTD) can be applied successfully for obtaining diffracted field from electrically large metal scatterers [3], but not from dielectric ones. It is because of reliable canonical dielectric wedge problems have not been solved yet. Therefore, we shall utilize the Kirchhoff approximation.

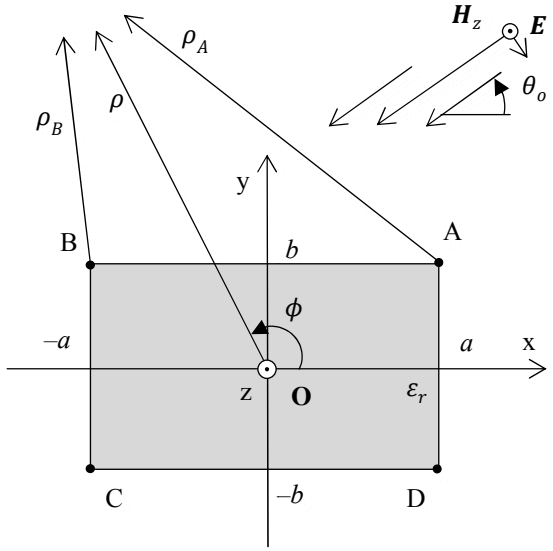

Fig. 1. Configuration of the problem

According to the field equivalent theorem [4], the scattering field from a body can be evaluated by radiation from equivalent current sources on a postulated surface enclosing the body. By taking this surface at plane $y = b$, the scattered field for $y > b$ may be evaluated via equivalent electric and magnetic currents, namely $\boldsymbol{J}$ and $\boldsymbol{M}$.

These currents may be given approximately by the reflected plane wave:

$$H_z^r = \Gamma(\theta_0)e^{-ikx\cos\theta_0+i(y-2b)\sin\theta_0} \quad (2)$$

via $\boldsymbol{J} = \hat{\boldsymbol{n}} \times \boldsymbol{H^r}$ and $\boldsymbol{M} = \boldsymbol{E^r} \times \hat{\boldsymbol{n}}$, with $\hat{\boldsymbol{n}}$ denotes the normal unit vector to the surface, and $\Gamma(\theta_0)$ is the corresponding plane wave reflection coefficient at the interface $y = b$, and is given by

$$\Gamma(\theta_0) = \frac{\varepsilon_r \sin\theta_0 + \sqrt{\varepsilon_r - \cos^2\theta_0}}{\varepsilon_r \sin\theta_0 - \sqrt{\varepsilon_r - \cos^2\theta_0}}. \quad (3)$$

Thus the equivalent currents $\boldsymbol{J}$ and $\boldsymbol{M}$ on the plane ($y = b, -a \leq x \leq a$) may be given by

$$J_x = \Gamma(\theta_0)e^{-ikb\sin\theta_0}e^{-ikx\cos\theta_0}, \quad (4)$$

$$M_z = -Z\sin\theta_0\,\Gamma(\theta_0)e^{-ikb\sin\theta_0}e^{-ikx\cos\theta_0}, \quad (5)$$

where $Z = \sqrt{\mu_0/\varepsilon_0}$ is the free space wave impedance.
The scattered field $H_z^s (= H_1^s + H_2^s)$ in the upper half plane ($y > b$) can be calculated by integrating the radiation contribution from the above currents as

$$H_1^s = \frac{-i}{4}\int_{-a}^{a} J_x(x_0) \cdot \frac{\partial}{\partial y} H_0^{(1)}\left(k\sqrt{(x-x_0)^2+(y-b)^2}\right) dx_0, \quad (6)$$

$$H_2^s = \frac{\omega\varepsilon}{4}\int_{-a}^{a} M_z(x_0) \cdot H_0^{(1)}\left(k\sqrt{(x-x_0)^2+(y-b)^2}\right) dx_0, \quad (7)$$

where $H_0^{(1)}(\chi)$ denotes the zero-th order of the Hankel function of the first kind. The spectral representation of the Hankel function:

$$H_0^{(1)}(x,y;x_0y_0) = \frac{1}{\pi}\int_{-\infty}^{\infty} \frac{e^{i\xi(x-x_0)+i\sqrt{k^2-\xi^2}|y-y_0|}}{\sqrt{k^2-\xi^2}} d\xi \quad (8)$$

may be used for Eqs.(6),(7) to get double integral form. Interchanging the order of the integration and executing the integration with respect to variable x_0, one gets

$$H_1^s = \frac{i}{4\pi}\Gamma(\theta_0)e^{-ikb\sin\theta_0-ika\cos\theta_0} \cdot \int_{-\infty}^{\infty} \frac{1}{(k\cos\theta_0+\xi)} e^{i\xi(x-a)+i\sqrt{k^2-\xi^2}(y-b)} d\xi - \frac{i}{4\pi}\Gamma(\theta_0)e^{-ikb\sin\theta_0+ika\cos\theta_0} \cdot \int_{-\infty}^{\infty} \frac{1}{(k\cos\theta_0+\xi)} e^{i\xi(x+a)+i\sqrt{k^2-\xi^2}(y-b)} d\xi, \quad (9)$$

$$H_2^s = \frac{ik\sin\theta_0}{4\pi}\Gamma(\theta_0)e^{-ikb\sin\theta_0-ika\cos\theta_0} \cdot \int_{-\infty}^{\infty} \frac{1}{(k\cos\theta_0+\xi)} e^{i\xi(x-a)+i\sqrt{k^2-\xi^2}(y-b)} d\xi - \frac{ik\sin\theta_0}{4\pi}\Gamma(\theta_0)e^{-ikb\sin\theta_0+ika\cos\theta_0} \cdot \int_{-\infty}^{\infty} \frac{1}{(k\cos\theta_0+\xi)} e^{i\xi(x+a)+i\sqrt{k^2-\xi^2}(y-b)} d\xi. \quad (10)$$

When the saddle point technique is applied to evaluate the integral for far field, there is a pole singularity at $\xi = -k\cos\theta_0$, whose residue recovers the reflected plane wave contribution in Eq.(2), while each saddle point contribution gives us diffracted field. These fields may be combined to get

$$H_1^s \sim \frac{e^{ik\rho+i\frac{\pi}{4}}}{2\sqrt{2\pi k\rho}} \frac{\sin\theta_0}{\cos\theta_0+\cos\phi}\Gamma(\theta_0) \cdot e^{-ik(a\cos\theta_0+b\sin\theta_0)}e^{-ik(a\cos\phi+b\sin\phi)} - \frac{e^{ik\rho+i\frac{\pi}{4}}}{2\sqrt{2\pi k\rho}} \frac{\sin\theta_0}{\cos\theta_0+\cos\phi}\Gamma(\theta_0) \cdot e^{-ik(-a\cos\theta_0+b\sin\theta_0)}e^{-ik(-a\cos\phi+b\sin\phi)}, \quad (11)$$

$$H_2^s \sim \frac{e^{ik\rho+i\frac{\pi}{4}}}{2\sqrt{2\pi k\rho}} \frac{\sin\phi}{\cos\theta_0+\cos\phi}\Gamma(\theta_0) \cdot e^{-ik(a\cos\theta_0+b\sin\theta_0)}e^{-ik(a\cos\phi+b\sin\phi)} - \frac{e^{ik\rho+i\frac{\pi}{4}}}{2\sqrt{2\pi k\rho}} \frac{\sin\phi}{\cos\theta_0+\cos\phi}\Gamma(\theta_0) \cdot e^{-ik(-a\cos\theta_0+b\sin\theta_0)}e^{-ik(-a\cos\phi+b\sin\phi)}, \quad (12)$$

for far field ($k\rho >> 1$). One may note that the contribution from the singularity is not needed for far field approximation and the singular behavior at the specular reflection direction ($\phi = \pi - \theta_0$) of the fields in Eqs.(11), (12) cancels each other to obtain as

$$H^s = H_1^s + H_2^s = -i4ka\sin\theta_0 \frac{e^{ik\rho+i\frac{\pi}{4}}}{2\sqrt{2\pi k\rho}}\Gamma(\theta_0)e^{-i2kb\sin\theta_0}. \quad (13)$$

Formulation can also be applied for the scattering from other side of the illuminated polygonal surface. Thus, the total scattering field could be a summation of contribution by two lit surfaces.

Two dimensional radar cross section (echo width) σ_{2D} may be calculated from

$$\sigma_{2D} = \lim_{n\to\infty} 2\pi\rho|H^s|^2, \quad (14)$$

and the corresponding three dimensional radar cross section σ_{3D} in the case of normal incidence to the cylindrical axis can be estimated approximately from the above σ_{2D} via [5]

$$\sigma_{3D} = \frac{2L^2}{\lambda}\sigma_{2D}\,, \qquad (15)$$

where L denotes the axial length of the cylindrical body.

III. Numerical Results And Discussions

In order to show the validity of our analytical formulation derived here, monostatic RCS σ_{3D} has been calculated and compared with the corresponding measurement values [6, 7]. Three models are used for comparison and Table I shows their dimensions and their permittivity which are measured by probing method [6].

TABLE I
List of Models And Their Permittivity

Name	Parameters		
	Dimensions $2a\times 2b\times L$ [mm]	**Freq.** f [GHz]	**Relative permittivity** ε_r
Model 1	80×80×80	18	Metal
		24	Metal
Model 2	80×80×80	18	6.5114+i 0.0852
		25	6.9091+i 0.1364
Model 3	100×40×100	18	6.5850+i 0.0909

Figures 2 and 3 are results of monostatic calculation for Model 1 which is made of metal facets. Thus, the reflection coefficient becomes $\Gamma(\theta_0) = +1$ for any incident angle $\theta_0$at any frequency. Figure 2 is for 18GHz, while Fig.3 is for 24 GHz. Four distinctive peaks of the same maximum value are observed in 90-degree angular period in both figures. Peak RCS value, which is due to the specular reflection direction of the facets, is approximately obtained from Eqs.(13) and (15) with $\phi = \theta_0 = \pi/2$. Then one gets

$$\sigma_{3D} = \frac{16\pi a^2L^2}{\lambda^2}\left|\Gamma(\theta_0 = \frac{\pi}{2})\right|^2 = \frac{16\pi a^2L^2}{\lambda^2}, \qquad (16)$$

which becomes 2.68 dBsm at f=18GHz, and 7.22 dBsm at f= 24GHz. Our analytical estimation compared very well with measurement values for both frequencies not only for the peaks at specular reflection angles ($\phi = 0^o, 90^o, 180^o, 270^o$), but also for minor lobes. This observation matches with the fact that the Kirchhoff approximation is rather accurate in the vicinity of the shadow boundaries, since the pole singularity correctly predicts the incident and reflected plane wave spectra in the spectral domain integral representation in Eqs.(9) and (10).

RCS from lossy dielectric cubes are also calculated and compared with measured data of Models 2 and 3, as shown in Figs.4 ~ 6. Model 2 is made of synthetic rubber sheets which show frequency dispersive characteristics. Therefore, the permittivity is frequency dependent. One observes that the specular RCS peaks and its main lobes can be predicted well by our formula, while rather strong RCS values (about −20 dBsm) are found in the measurement data. This discrepancy may be caused by the multiple bouncing fields returned from the bottom surface, which are omitted in our formula.

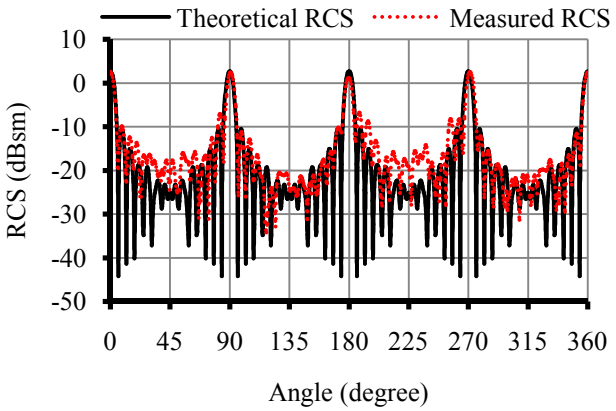

Fig. 2. 3D monostatic RCS of Model 1 (a metal rectangular cube), 18GHz.

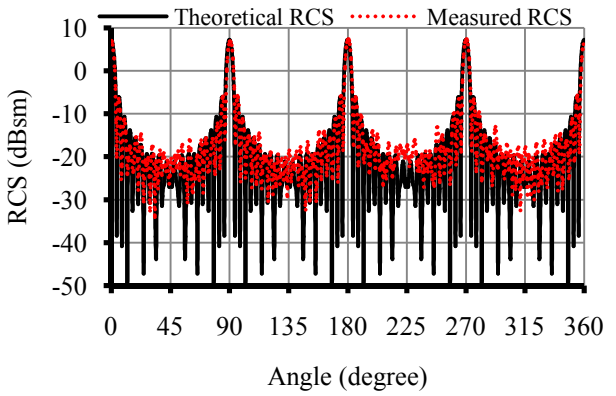

Fig. 3. 3D monostatic RCS of Model 1 (a metallic rectangular cube), 24GHz.

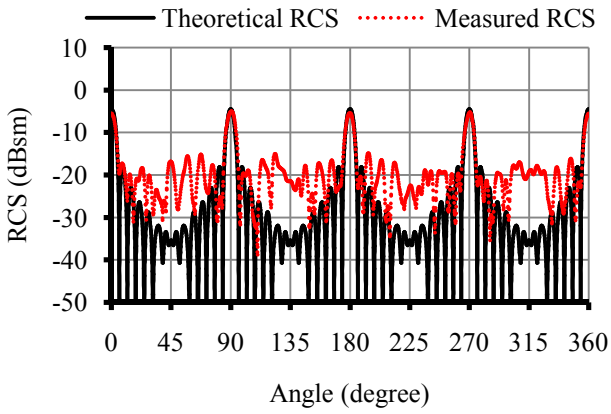

Fig. 4. 3D monostatic RCS of Model 2 (a rubber rectangular cube), 18GHz.

These multiple transmitted fields would become damped due to the lossy nature of the material, but it sometimes gives us unexpected contributions to the monostatic observation directions.

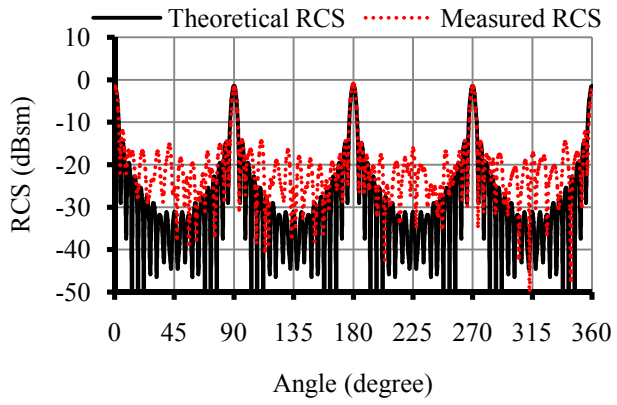

Fig. 5. 3D monostatic RCS of Model 2 (a rubber rectangular cube), 25GHz.

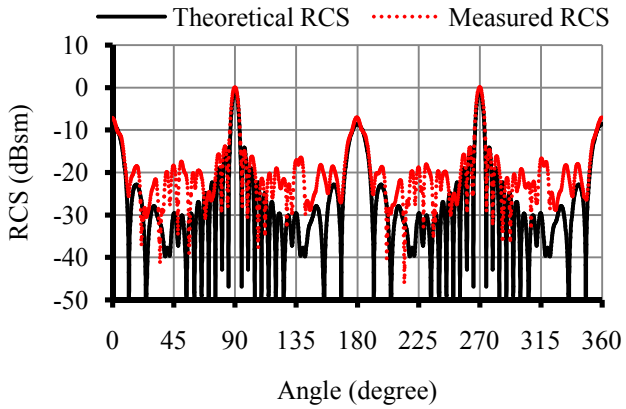

Fig. 6. 3D monostatic RCS of Model 3 (a rubber rectangular cube), 18GHz.

IV. Conclusion

In this paper, the scattering from lossy rectangular cylinders has been estimated by high frequency technique, on the assumption that the objects are large in comparison with the operating wavelength. Kirchhoff approximation is applied to obtain the equivalent current distribution on the surface of the scatterer, and then the scattered fields are calculated by integrating the radiation field from these equivalent current sources.

Numerical calculation has been done for the prediction of monostatic RCS values, and these values are compared with measured data. Three models are used and good agreement has been observed, especially for specular reflection directions. Since these specular reflection returns contain targets' information, such as size and the constitutive electric constant, the target reconstruction may be possible as we did for metal scatterers [8]. This aspect shall be pursued in the future.

Acknowledgment

This research was partially supported by the Scientific Research Grant-In-Aid (24560478, 2012) from JSPS (Japan Society for the Promotion of Science), Japan.

References

[1] E. F. Knott, J. F. Shaeffer, M. T. Tuley, *Radar Cross Section*, 2nd ed, Massachusetts, USA: Artech House, 1993

[2] E. F. Knott, *Radar Cross Section Measurements*, New York, USA: Van Nostrand Reinhold, 1993

[3] J. B. Keller, "Geometrical Theory of Diffraction," *JOSA*, Vol. 52, no. 2, pp. 116–130, 1962.

[4] R. F. Harrington, *Time-Harmonic Electromagnetic Fields*, McGraw-Hill Co., 1961.

[5] R. A. Ross, "Radar cross section of rectangular flat plates as a function of aspect angle," *IEEE Transaction on Antennas and Propagation*, vol. AP-14, no. 3, pp. 329–335, May, 1966.

[6] M. Ishikawa and H. Shirai, "Non-contacting estimation of complex permittivity using RCS measurement," *Proc. ISAP2009*, pp. 588–591, 2009.

[7] S. Kojima, M. Ishikawa, and H. Shirai, "A study on estimation method of complex permittivity using radar cross section," *IEEJ Tech. Rep.* EMT-08-09, pp. 1–6, 2008 (in Japanese).

[8] H. Shirai, Y. Hiramatsu and M. Suzuki, "Reconstruction of polygonal cylindrical targets with curved surfaces from their monostatic RCS," *IEICE Transactions on Electronics*, E88-C (12), pp. 2289–2294, 2005.